Simulation of Combustion Systems with Realistic *g*-jitter

final progress report

Principal Investigator:
William E. Mell
Research Assistant Prof.
Department of Mechanical Engineering
1495 East 100 South
109 Kennecott Research Building
University of Utah
Salt Lake City, UT 84112
(801)585-6861
(801)585-1456 (fax)
ruddy@eng.utah.edu

Co–Investigators:
Dr. Kevin B. McGrattan
Dr. Howard R. Baum
Building and Fire Research Lab.
National Institute of Standards and Technology
Gaithersburg, MD

Period of performance:~ March 23, 2000 – March 22, 2003
Award No.: NAG3-2403

Table of Contents

1 Project Overview

In this project a transient, fully three-dimensional computer simulation code was developed to simulate the effects of realistic *g*–jitter on a number of combustion systems. The simulation code is capable of simulating flame spread on a solid and nonpremixed or premixed gaseous combustion in nonturbulent flow with simple combustion models. Simple combustion models were used to preserve computational efficiency since this is meant to be an engineering code. Also, the use of sophisticated turbulence models was not pursued (a simple Smagorinsky type model can be implemented if deemed appropriate) because if flow velocities are large enough for turbulence to develop in a reduced gravity combustion scenario it is unlikely that g-jitter disturbances (in NASA's reduced gravity facilities) will play an important role in the flame dynamics. Acceleration disturbances of realistic orientation, magnitude, and time dependence can be easily included in the simulation.

The simulation algorithm was based on techniques used in an existing large eddy simulation code which has successfully simulated fire dynamics in complex domains. This technique is very efficient computationally so that simulations of the entire experimental domain with one to two million grid cells can be performed on current single processor workstations. An efficient cell blocking method allows the user to easily define and modify the solid surfaces comprising the simulation domain and diagnostic equipment. As state above, to preserve computational efficiency, simple combustion models was used (e.g., flame sheet or highly reduced, finite rate, second order, global Arrhenius kinetics). A multiblocked grid approach was implemented to allow regions requiring high resolution (i.e., the flame) to be covered by a fine grid while coarser grids cover the rest of the experimental volume.

The final computer simulation code has resulted from incorporating parts of a microgravity flame spread code into NIST's fire simulation code (called Fire Dynamics Simulator, FDS). Each of these codes has been in separate development for years at NIST but this approach has allowed the microgravity code development to leverage off the fire code development. For example, the visualization software package Smokeview, developed at NIST, can be used.

Acceleration disturbances or *g*–jitter about the background level of reduced gravity exist in all the microgravity facilities. Low frequency *g*–jitter has been repeatedly observed to disturb a number of combustion systems. Guidelines regarding tolerable levels of acceleration disturbances for a given combustion system (i.e., flame balls, gas jet diffusion flames, etc.) have been developed for use in the design of ISS experiments. The validity of these guidelines, however, remains largely unknown and untested. The simulation code developed in this project allows users to assess the *g*-jitter effects on their flame for the microgravity facility in question. This can help investigators plan experiments and interpret their data. For example on the ISS an acceptable acceleration environment could be achieved through the combined use of a passive isolation system and scheduling appropriate crew/station activity (e.g., no ergometer exercise). Different flames are expected to have different acceleration environment requirements and, therefore, demands on crew/station activity. The simulation code provides one means of determining these requirements.

2 Overview of simulation code at the project's end

An overview of the capabilities and technical approach of the computer simulation approach at the end of the project are listed below. For more detailed information on the technical approach see McGrattan *et al.* (2002) or Mell *et al.* (2003b)

- Conservation equations for total mass, momentum and species mass fractions are solved numerically. A constraint on the divergence of the velocity, derived by coupling the conservation equations for energy [in the low Mach number thermally, expandable limit (Rehm and Baum, 1978)] and total mass (using the equation of state for ideal gases), is used whenever the velocity divergence is present.
- A Poisson equation for the hydrodynamic pressure (obtained by taking the divergence of the momentum equation) is solved using a fast direct solver. This results in improved stability and computational efficiency over iterative solvers (such as algebraic multigrid).
- The numerical approach uses fully explicit second-order Runge Kutta time stepping, with second order spatial discretization and partial upwinding on a staggered grid to obtain a time dependent solution to the governing equations.
- The computational grid can be three-dimensional (with stretching in at most two directions), two-dimensional (with no stretching), or axially-symmetric. Multiple grids each with a different grid resolution can be used to focus higher resolution grid in the volume containing the flame and coarser grids in the remaining volume comprising the experimental domain. The computational grid cells must be rectilinear in shape. This restriction is due to the use of the fast direct solver.
- It is possible to run either direct numerical simulations (DNS) in which molecular values of the transport coefficients are used, or large eddy simulations (LES) in which the viscous dissipation is modeled following Smagorinsky and the conductivity and diffusion coefficients are determined from the Prandtl and Schmidt numbers respectively.
- Combustion models:
  - limited to a single hydrocarbon fuel.
    [CxHyOz] + vO2 [O2] -> vH2O [H2O] + vCO2 [CO2] + vCO [CO] + vsoot [soot]
  - mixture fraction based infinite chemistry
  - global one-step, Arrhenius kinetics for sufficiently high resolution grids (DNS)
- Thermal radiation
  - finite volume solver
  - fully implemented for the mixture fraction combustion model
  - not implemented for the finite rate combustion model
  - grey gas, or
  - band averaged (default is 6 bands for CO2 and H20, up to 3 more bands can be added if fuel is a relevant absorber)
  - absorption coefficient(s) are tabulated as functions of mixture fraction and temperature using a narrow-band model RADCAL (Grosshander, 1993)
- Boundary conditions: forced flow, passive (open), solid, symmetry plane(s)

- Solid objects are easily included with the computational domain (to simulate the effects of experimental structures)
- Time resolved, measured acceleration vector can be used to represent the ambient acceleration environment.
- Scenarios of flame suppression (by gaseous agents (e.g., CO2) or water droplets) can be investigated when the finite rate combustion model is used.
- Public domain companion visualization software package, Smokeview, developed by Glenn Forney of the National Institute of Standards and Technology (NIST) (Forney, 2003). Smokeview can display slice planes of color contours representing the values of a given variables. Flow vectors and isosurfaces are also possible. All of which can be animated and output frame by frame in jpeg or png format.
- Source code is portable to Windows (98,2000,NT), Linux, and UNIX (IRIX,Solaris) operating systems.
- Code is written in Fortran 90 and developed for single processor machines.

3 Examples of the simulation's capabilities

The following examples are meant to illustrate the capabilities of the simulation code. In most cases they are from exploratory simulations. Results from a more thorough testing and validation of the simulation are given in Sec. 4 below for the case of spherical diffusion flames. The following discussion and animations can be found on a webpage devoted to this project Mell *et al.* (2003a).

3.1 GIFFTS for S-Flame Experiments

The Gravitational Influences on Flammability and Flame spread Test System (GIFFTS) rig is used to generate spherical diffusion flames. The rig contains a 21 liter cylindrical combustion chamber (25.4 cm [10 in] diameter, 53.34 cm [21 in] tall). Simulations of this volume approximated as a 25 cm wide, 25 cm deep, and 50 cm tall rectangular volume were conducted. Figure 1 shows the stoichiometric surface of the flame and color contours of radiative flux on the solid walls of the experimental enclosure at $t = 10$ s. The experimental structure for supporting the 12 mm cubic burner can also be seen (except for the fuel supply rod which had dimensions below the grid resolution). The flame is created by a mixture of 10% hydrogen and 90% nitrogen (by mass fraction) injected into standard air from a 12 mm on a side cubic burner. The net radiative flux is largest (~0.75 kW/m^2) on the rectangular support surface located 10 cm from the center of the burner. Over the time scale of the simulation this flux does not cause an appreciable change in the temperature of the support surface (this temperature is not shown). This example shows how experimental apparatus can be included in the simulation.

Figure 2a shows color contours of temperature from the same simulation of Fig. 1. In Fig. 2b the temperature contours are also shown but in this case no radiation solver was employed – the flame is adiabatic. The effects on flame structure/temperature are clear and reasonable. The case without

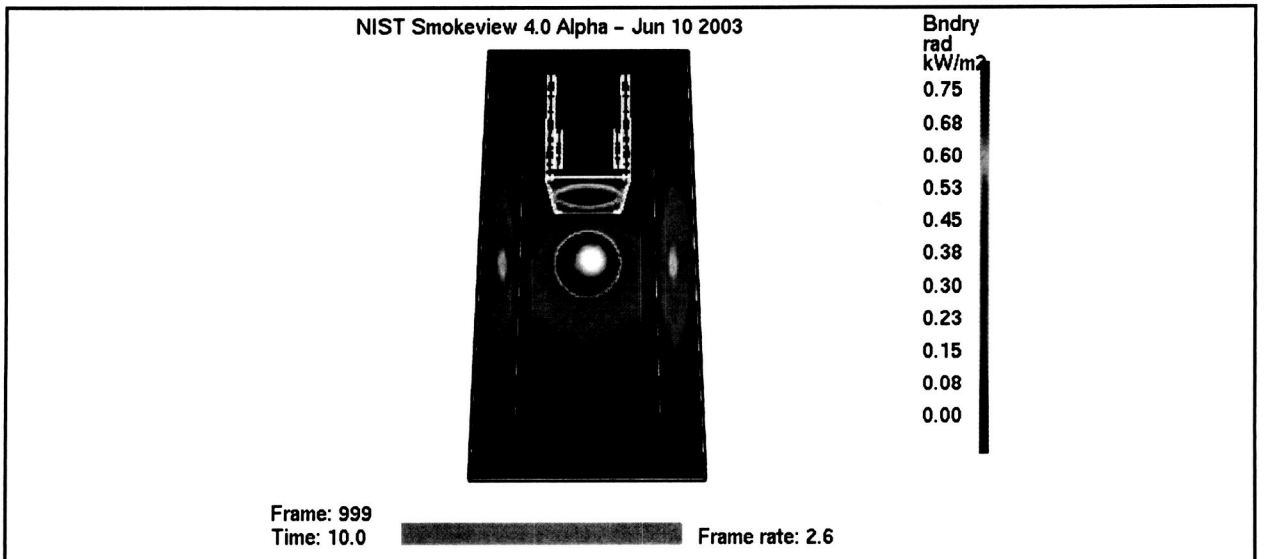

FIGURE 1: Isosurface of stoichiometric value of mixture fraction for a hydrogen/nitrogen fuel mixture exiting from a 12 mm cubic burner. Thermal radiation flux values on the walls of the enclosure are also shown with legend of flux values at right. This is a fully 3-D simulation which used the wide band finite volume radiation solver; 4 mm uniform grid; ~ 500,000 grid cells (64x64x128) over a 25 cm x 25 cm x 50 cm spatial domain. The full 10 s of simulated real time required 9.7 cpu hours (1482 time steps) with a 1.7 GHz Pentium 4 chip, Linux (Lahey V6.1 Fortran compiler). The spectral wide band radiation solution consumed 61% of the computational time.

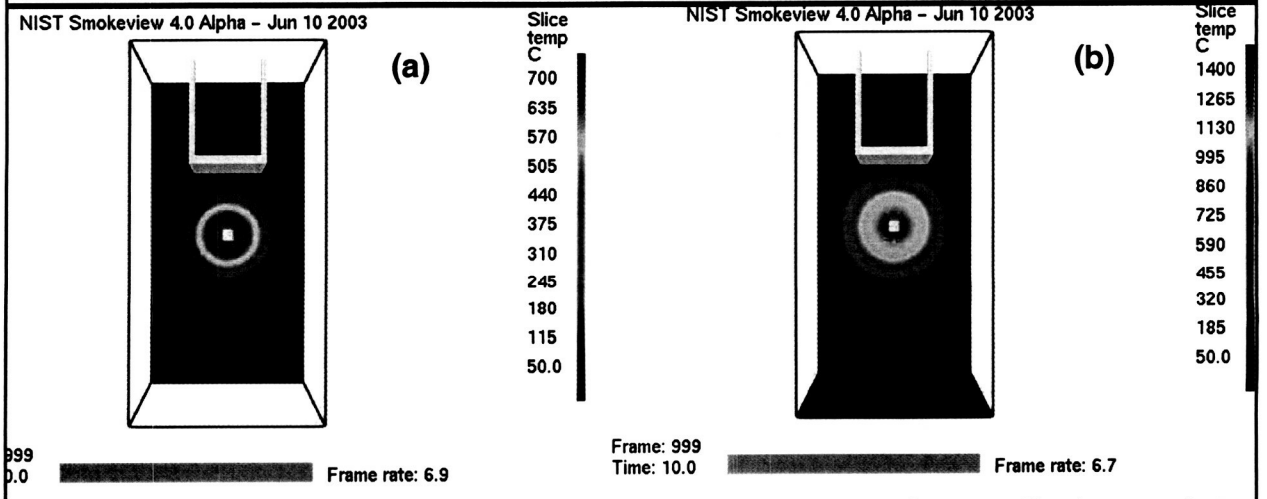

FIGURE 2: Color contours of temperature. **(a)** Same case as in Fig. 1. **(b)** Same as Fig. 1 except that no radiation solver is employed – flame is adiabatic with no radiative heat loss to the surroundings. Without the cost of the radiation solver the simulation required 4.7 cpu hours. Note the difference in the temperature scales between figures (a) and (b).

radiative transfer has peak temperatures which are higher and extend over a broader region since radiative heat loss to the surroundings does not occur. Note that the color legend on Fig. 2a is blue: 50 C to red: 700 C; the legend in Fig. 2b is 50 C to 1400 C.

3.2 Mist suppression of premixed propane/air.

The code is capable of simulating the effects of water droplets on heat and mass transfer. This is relevant to ongoing work funded by NASA to investigate the use of water mist as a suppressant. Acceleration disturbances may influence the distribution of a the droplets comprising a water mist and thereby influence the outcome of the experiment. A collaborative effort was began in the last year of the project with the NASA funded Water Mist Fire-Suppression Experiment (McKinnon *et al.*, 2003). Time constraints did not allow simulations to be made to assess the influence of an acceleration disturbance on droplet distribution. However, as an example of the simulation code's capability two examples of simulations with water droplets present in a premixed combustion scenario are given here.

Premixed propane/air in a 2-D chamber 6 cm high and 25.6 cm long was ignited at the left end (by heating the left wall). The right end was open to standard air. The combustion model was a single step, finite rate, reaction with Arrhenius kinetics. The kinetic constants were obtained from Westbrook and Dryer (1981). No acceleration disturbance was present, $g = 0$. Figure 3 shows the two

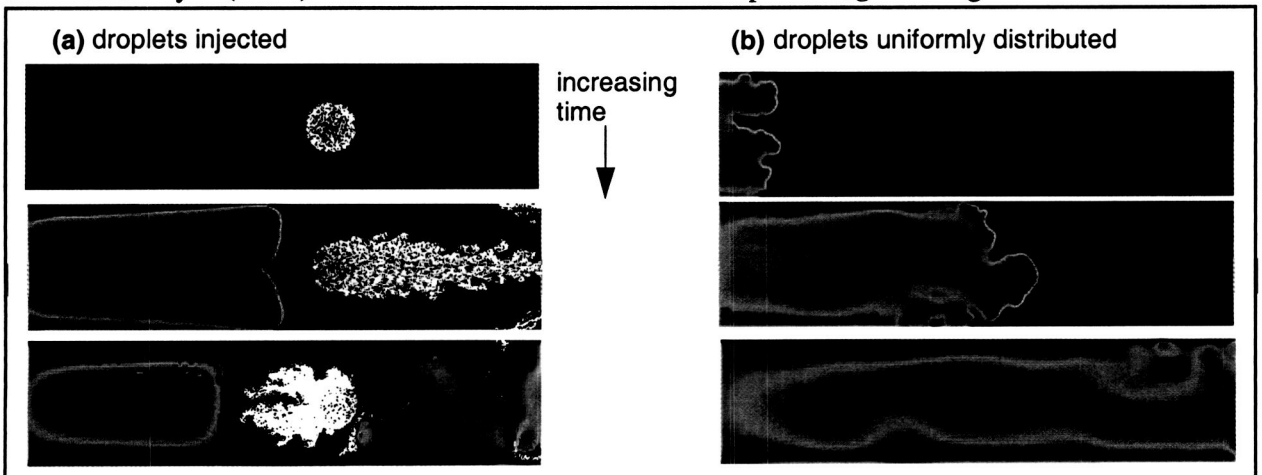

FIGURE 3: Color contours of temperature from a premixed propane/air flame igited at left boundary and spreading to the right. Water droplets are shown in figure (a). Top and bottom boundaries are solid and held at a fixed temperature of 20 C; the right boundary is open to ambient air. The 2-D simulation used 1mm grid, 256 x 60 uniform grid cells over a 25.6 cm long and 6 cm high domain. Required 23 cpu minutes for 3.7 s simulated real time on a R12000, 270 MHz SGI Octane.

cases considered: Fig. 3a in which droplets were injected into the domain, and Fig. 3b in which droplets were uniformly distributed throughout the domain. In Fig. 3a expansion from the premixed flame and evaporating droplets create a flow from left to right. The droplets extinguish the flame near the centerline. The convoluted flame shape in Fig. 3b show the effects of nonuniform heat loss and expansion due the droplets which are not uniform in radius.

3.3 Flame spread over thermally over a thermally thin solid

The code is capable of simulating flame spread over a thermally thin cellulosic solid. The models and numerical approach used were based on earlier work (Nakabe *et al.*, 1994; McGrattan *et al.*,

1996; Mell and Takashi, 1998; Mell *et al.*, 2000). Results of two flame spread simulations are shown in Figs. 4a,b. The cellulosic sample is defined to be plane of symmetry. Barring the effects

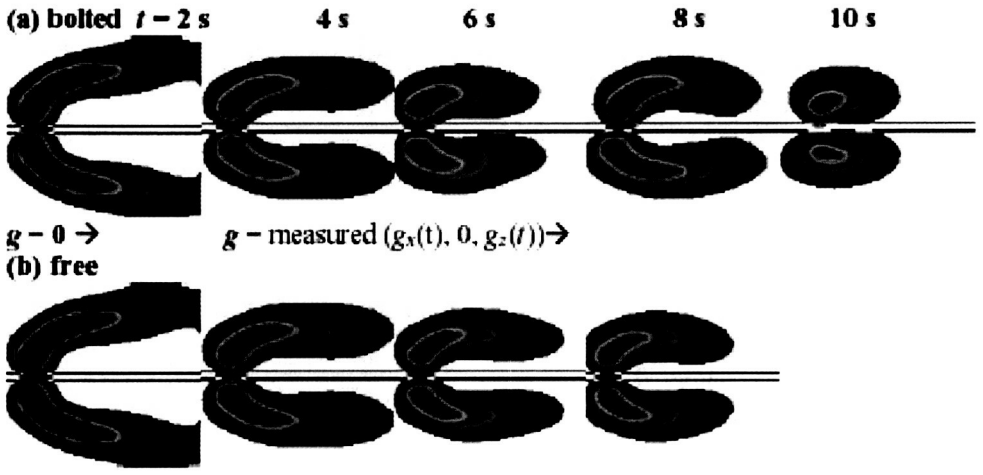

FIGURE 4: Time sequence of cross sections of heat release rate from a 2-D flame spread simulation. A 0.5 cm/s wind blows from left to right. Acceleration **g** = $[g_x(t), 0, g_z(t)]$ measured in a bolted-down (a) and a free- floated (b) experimental rig on the KC-135 aircraft were used. Times are t = 2 s, 4 s, 6 s, 8 s and 10 s. The acceleration vector was imposed starting at t = 6 s (after flame reached an approximate steady state). Case (b) is not shown at 10 s since low- g only lasted for 4 s in free- floated case. No affects of g-jitter are seen in the free- floated case (b). Flame quenched for case (a) at t = 11 s. Simulation used uniform grid resolution of 2/3 mm, domain size was 12 cm in the horizontal direction and 4 cm in the vertical half space.

of holes in the sample this is a reasonable assumption. In Figs. 4a,b the acceleration vector, **g** = $[g_x(t), 0, g_z(t)]$, is from measured acceleration levels in the KC-135 aircraft with the experimental rig bolted down (Fig. 4a) and free floated (Fig. 4b). In both figures an ambient 0.5 cm/s wind blows from left to right. Acceleration levels in the free floated experiments are approximately two orders of magnitude lower (~ 5 x $10^{-4} g_E$, where g_E is normal gravity) than for the bolted down experiments. As a result, the flame is unaffected by the g-jitter in the free floated experiment. It should be noted that if the investigators wanted to measure steady state flame spread they may not choose the free-floated platform since reduced gravity lasts for only about 7 s – approximately to the time it takes for the simulated flame to reach steady state. Reduced gravity levels in the bolted down experiments last for 18 s to 20 s. But, as seen is Fig. 3a, g-jitter associated with the bolted down experiments affected the simulated flame and eventually caused it to extinguish at t= 11 s.

Acceleration disturbances are often analyzed using the power spectral densities derived from the the Fourier transform of the acceleration time history. This method allows one to determine if the disturbance can be characterized as occurring at certain frequencies. A possible representation of an acceleration is a sum of sine functions over the dominant frequencies. This representation, however, may not adequately represent the an acceleration disturbance in terms of its effect on a given combustion system – relative to the raw time history. This could occur, for example,

because not enough frequencies where used in the sum of sine functions. An example of this follows.

Figure 5a shows the power spectral density (PSD) of the g_z component of the acceleration

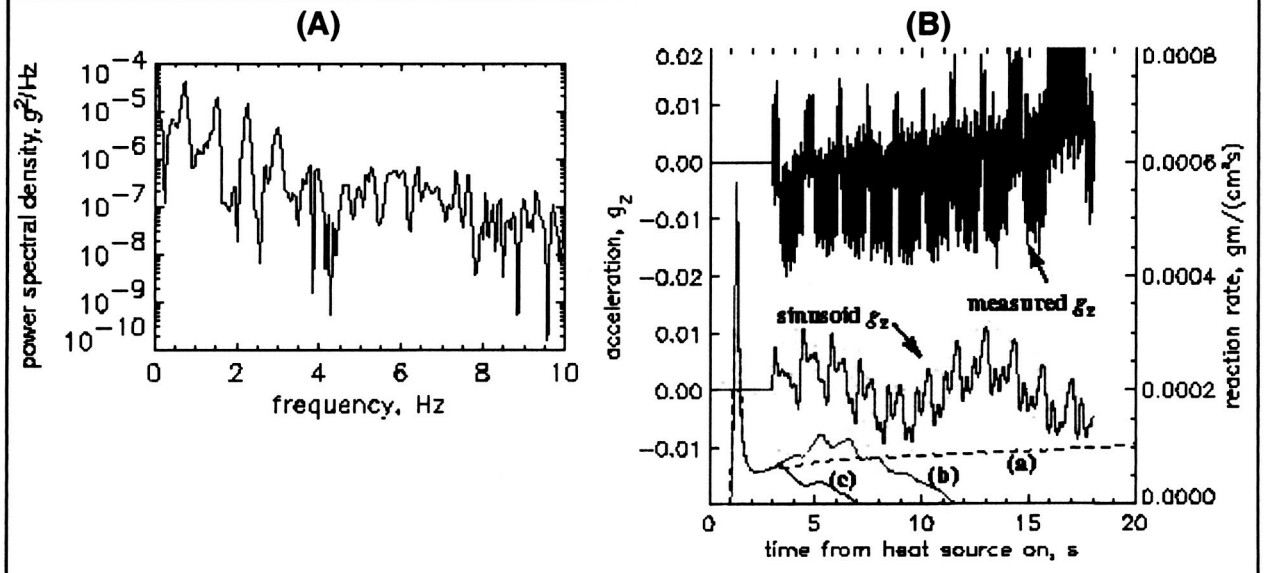

FIGURE 5: (A) Power spectral density of the gz component of the measured acceleration in a KC-135 aircraft. The measured raw gz is the top curve of figure (A). (B) Measured and sinusoid approximation of gz versus time from KC-135 bolted down experimental rig. Curves at the bottom of the figure show the reaction rates versus time from the 2-D flame spread simulation with (a) gz=0 [no disturbance]; (b) gz from sum of first five peaks in figure (A); (c) gz from experimental measurements.

vector associated with an experimental rig bolted to the frame of NASA's KC-135 aircraft. The measured time trace of g_z is the top curve in Fig. 5b. A possible approximate representation of g_z is a sum of sine functions. To obtain such a representation the first five peaks in the PSD were used to determine the frequencies and amplitudes of five sine functions. The amplitude associated with a given peak was found by integrating the PSD over a frequency band containing the peak. Two-dimensional simulations of upwind flame spread over a cellulosic sample were performed using three representations of the acceleration vector $\boldsymbol{g} = [0,0, g_z(t)]$: measured g_z , from a sum of five sinusoids (see Fig. 5b), or $g_z = 0$. Negative g_z pointed in the direction of flame spread. Note that the onset of nonzero g_z was delayed until the flame was established. In both cases with nonzero g_z the flame extinguished, but sooner for the measured g_z case. Clearly, the low frequency or transient behavior in the measured g_z was not adequately represented by the sum of sines.

4 Validation of the simulation for spherical diffusion flames

In this section the results of numerical simulations are compared to three separate spherical diffusion flame experiments. The reduced gravity NASA facilities used in the experiments considered

here were the 2.2 s drop tower, a free-floated experimental rig on a KC-135 aircraft, and a bolted-down experimental rig on a DC-9 aircraft. These facilities ranked in order of increasing acceleration disturbance are: drop tower, free-floated aircraft rig, and bolted-down aircraft rig. More extensive results of this validation effort can be found in Mell *et al.* (2003b).

4.1 Experiments in NASA's 2.2 s drop tower

Tse *et al.* (1999, 2001) conducted spherical diffusion flame experiments with hydrogen/methane/nitrogen fuel mixtures in NASA's 2.2 s drop tower. Highly resolved one-dimensional (assuming spherical symmetry) transient simulations with thermal radiation, detailed chemistry and transport were also conducted. The fuel gas mixture exited a 12.7 mm diameter porous sphere at different mass flows into atmospheric air. Results with various mass flow rates and fuel compositions were reported. The radius of a flame was measured as the distance from the center of the burner to the outer edge of the faint blue region of the flame. The flame was ignited in 1 g and allowed to burn for 1 s before the drop. Within 0.5 s after the drop became essentially spherical, suggesting the influence of acceleration disturbances on flame growth was negligible over the duration of the experiment. The same experiment was conducted in bolted-down and free-floated rigs on NASA's KC-135 aircraft. The reduced gravity was of longer duration in the aircraft, compared to the 2.2 s drop tower. However, the level of acceleration disturbance in both the bolted-down and the free-floated rigs significantly affected the flame shape (Tse, 2003).

Three-dimensional numerical simulations with the flame sheet mixture fraction based combustion model were made of an approximation to the drop tower experiments. Instead of a hydrogen/methane/nitrogen fuel mixture the simulations, which are limited to a single fuel, used a fuel mixture of 60%H_2-40%N_2 (by mole fraction). The hydrogen/nitrogen fuel mixture was ejected into standard air from a cube approximately 12.7 mm in width; the velocity of the fuel mixture injection was such that the fuel mass flow rate matched the experimental values. Three fuel mixture mass flow rate cases were considered: 0.00496 g/s, 0.0081 g/s, 0.013 g/s. During the initial 1 s of the simulation the ambient acceleration vector was the same as in the pre-drop stage of the experiment: $\boldsymbol{g}= (0,0,-g_e)$. This orientation of $\boldsymbol{g}$ allowed symmetry to be assumed across the $x = 0$ and $y = 0$ planes, resulting in a computational volume that was a quarter of the complete volume. Unless otherwise stated the results reported here used a computational domain of 0 cm <= x,y <= 7.5 cm and -7.5 cm <= z 7.5 cm; 64 grid points spanned the x and y directions and 128 in the z direction; the grid was uniform in all three directions. A number of runs were made with higher grid resolutions and larger domains to ensure that the results reported here were grid and boundary independent. The radius of the simulated flame in each coordinate direction was determined from the position of the peak chemical heat release rate. Using the peak temperature gave essentially the same result as can be seen from figures of profiles of heat release rate per unit volume and temperature.

After an initial 0.5 s period of full gravity in the simulations, the ambient acceleration was assumed to linearly change from $\boldsymbol{g} = (0,0,-g_e)$ to $\boldsymbol{g} = (0,0,0)$. This approximated the transition from full gravity to near microgravity when the experimental rig is released in the drop tower. The

time origin in the figures and discussion below is defined to be at the initiation of the ``drop". If the time history of $\boldsymbol{g}$ had been measured experimentally it could have been used in the simulation. However, these measurements are not routinely made in the NASA 2.2 s drop tower largely due to the prohibitive cost and the calibration effort required (Baumann, 2003).

Figure 6 shows the time history of the sphericity and concentricity of the simulated flame (they

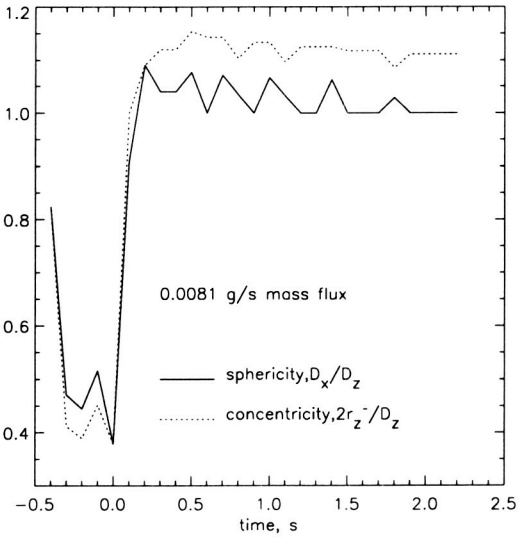

FIGURE 6: Time history of sphericity and concentricity for the mass flow rate case of 0.0081g/s. Experimental values are 1.0 and 0.94 at t = 0.5 s.

were computed every 0.1 s) for a mass flow rate of 0.081 g/s. Tse *et al.* (1999, 2001) found that for this fuel mass flow rate the flame had 1.0 sphericity and 0.94 concentricity at t = 0.5 s. Sphericity is defined as the ratio of the horizontal over the vertical diameters of the flame, D_x / D_z; concentricity is the ratio of twice the distance between the center of the burner over the vertical diameter of the flame, $2r^-_z$ / D_z (Miyasaka, 1981). The sphericity and concentricity of the simulated flame is in reasonable agreement with experimental values. The results in Fig. 6 were obtained with radiation transfer computed using a wide band model. Simulations without radiation transfer gave similar values of sphericity and concentricity. Note that in simulations with $\boldsymbol{g}$ = 0 (i.e., there was no initial period of normal gravity) both the sphericity and concentricity equaled 1.0 as they should.

Figure 7 shows the flame diameter versus time from both the drop tower experiments (solid symbols) and the numerical simulations (open symbols connected by lines) for the three different fuel mass flow rates considered. Diameters in both the simulation and experiment were measured across the flame in the horizontal direction (i.e., perpendicular to the direction of gravity). Overall the simulation provides reasonably good predictions of flame growth especially considering the simple combustion model employed (e.g., no differential diffusion, single fuel). The magnitude of the disagreement between simulation and experimental flame diameters at larger times is similar to that reported by Tse *et al.* (2001). However, their simulation contained more of the relevant

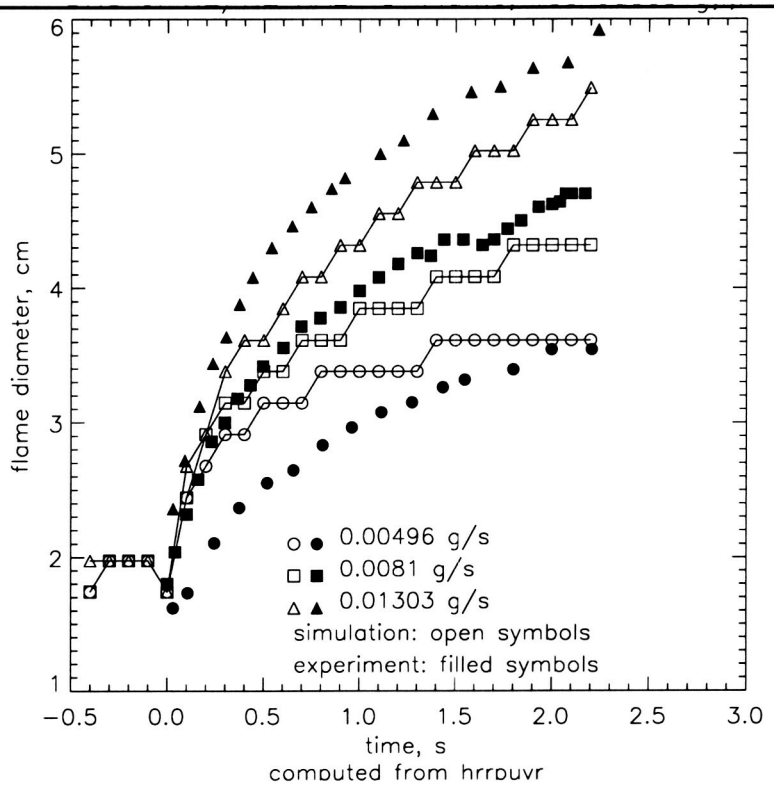

FIGURE 7: Flame diameter versus time from 3-D simulations (open symbols connected by lines) and experimental measurements (filled symbols). Experiments were conducted in NASA's 2.2 s drop tower facility. During an initial 0.5 s period the flame is subjected to normal gravity.

physics (differential diffusion, complex chemistry). For this reason their simulations of the small mass flow rate case are in better agreement with the experiments at earlier times. Flame diameter predictions from simulations without radiation transfer give essentially the same results for the 0.0081 g/s and 0.01303 g/s mass flow rate cases; for the smallest mass flow rate case the adiabatic simulations give larger flame diameters (this and other results are more fully covered in Mell *et al.* (2003b)).

Next, simulation predictions will be compared to experimental results in conditions of larger acceleration disturbances.

4.2 Experiments in NASA's free-floating rigs in a KC-139 aircraft

Recent KC-135 aircraft experiments reported by Feikema (2001) found that the free-floated experiments of spherical diffusion flames suffered from g-jitter effects. The source of the disturbance was believed to be due to aerodynamic drag which introduced a constant 5 milli-g disturbance, $\boldsymbol{g} = (0.005, 0, 0.005)g_e$; this is an order of magnitude larger than in the DC-9 free-floated experiments. Vibratory levels in the KC-135 were of significantly smaller magnitude, 50 micro-g.

Based on this experiment the acceleration vector was assumed to be of the form $\boldsymbol{g} = (g_x, 0, g_z)$. This allowed the simulation to be run with a symmetry plane along y = 0. The level of acceleration used was $g_x = g_z = 0.005 g_e$. This level of acceleration was imposed at time zero. Figure 8

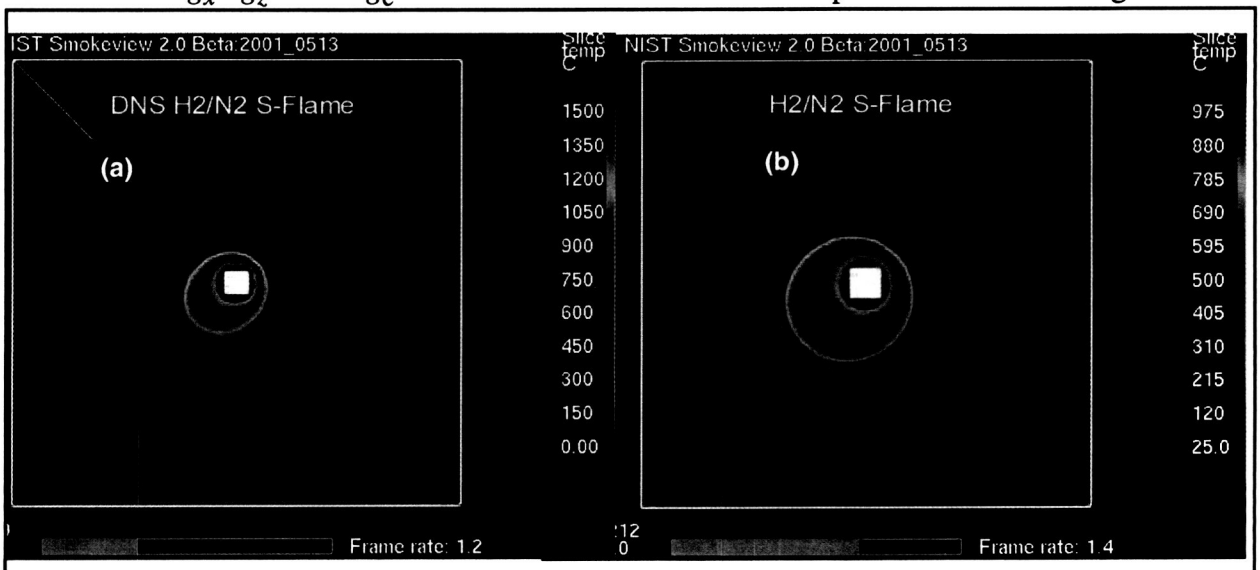

FIGURE 8: Temperature contours from 3-D simulations of a hydrogen flame, at $t = 1$ s, with a constant acceleration vector $\boldsymbol{g} = (0.005, 0, 0.0005) g_e$. In these figures the coordinate directions $x < 0$ and $x > 0$ are left and right, respectively; $y < 0$ is toward the reader; $z < 0$ and $z > 0$ are down and up, respectively. Spatial dimensions of computational domain were 15 cm x 7.5 cm x 15 cm. **(a)** Well resolved direct numerical simulation with 1.2 mm uniform grids, 128x64x128 grid cells; 10 cpu hours needed for 1.4s on 1.7 GHz P4. **(b)** Coarse grid 3.75 mm, 40x20x40 grid cells; 9 cup min for 1.4 s on 450 MHz P3.

shows the results of the 3-D simulations of a H_2/N_2 fuel mixture (0.1, 0.9 mass fraction level, respectively) vented from the surface of a 12 mm cube (this cube can be seen in the center of the figures). The fast chemistry mixture fraction based combustion model was used. Results from two different grid resolutions are shown. In Fig. 8a uniform grid cell of 1.2 mm were used; in Fig. 8b the resolution is 3.75 mm. This level of constant acceleration ($g_x = g_z = 0.005 g_e$.for 1 s, g_y=0) clearly causes the flame to lose spherical symmetry –consistent with the experimental finding of Feikema (2001).

4.3 Experiments in NASA's bolted-down rigs in a DC-9 aircraft

Struk *et al.* (1996) measured variations in the gravity level aboard NASA Lewis Research Center's DC-9 aircraft for experimental rigs which were either attached to the frame of the aircraft or free–floated. As shown in Fig. 9, for experiments attached to the airframe during the time interval $t = 4$ - 13 s reduced g levels oscillated between ± 0.02 g_e along the vertical axis (ceiling to floor, g_z), 0.0 to - 0.01 g_e along the lateral axis (wing–tip to wing–tip, g_y) and remained steady at – 0.01 g_e along the longitudinal axis (g_x); total reduced gravity level duration was 18 s to 20 s. Here g_e is normal gravity. For the free-floated experiments the acceleration level was much smaller,

between $\pm 5 \cdot 10^{-4}$ g_e along each of the axes (not shown). However, reduced gravity levels lasted for only a maximum of 7 s since time was spent positioning the experimental rig.

Droplets of various sizes were burned by Struk *et al.* (1996) to test the hypothesis of a large diameter extinction limit. Results from the experiment and the 3-D transient simulation code (using the measured $g_{x,y,z}/g_e$ in Fig. 9) are shown in Fig. 10. Individual frames from a video recording of the

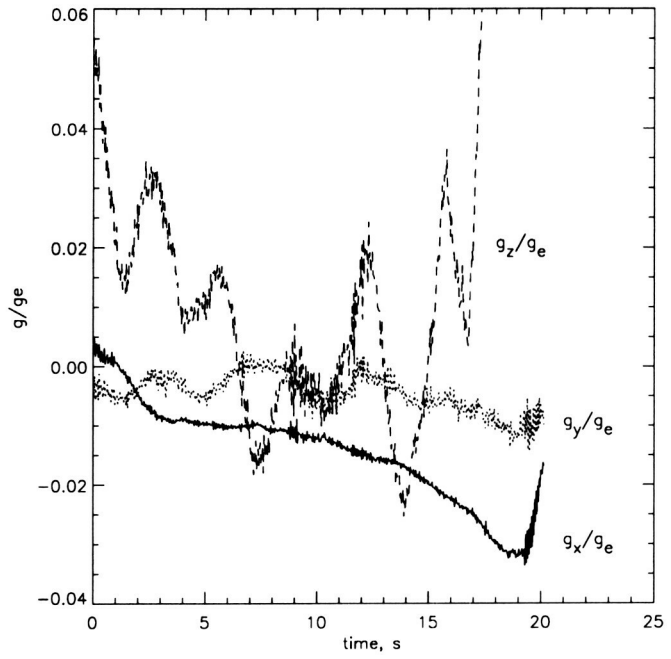

FIGURE 9: Time history of the measured components of the acceleration vector in the bolted-down spherical diffusion flame experiments of Struk *et al.* (1996) conducted on NASA's DC-9 aircraft.

experimental droplet flame are shown on the left; frames at the same times from animations of two isosurfaces of simulated temperature are shown on the right. The simulation tracked very closely the influence of acceleration disturbances, including the lag in flame response to changes in the orientation of the disturbance. It is clear from Fig. 10 that *g*–jitter effects corrupted the experiments which were attached to the airframe. Both increased soot production and non-spherical flame shapes were associated with *g*–jitter. Fortunately, the time period of the less disturbed free-floating experiments was sufficiently long for visible flame extinction to be observed – in support of a large diameter extinction limit. Simulations, not shown here, with accelerations measured from the free-floated experiments predicted the flame would be unaffected.

The liquid/gas conversion present in the experiments was not accounted for in the simulations. Instead, gas was vented directly from a cube located in the center of the computational domain. Both the composition of the gas and the size of the cube was varied to investigate a number of issues. For, example it was found that relatively cheap simulations with a light, isothermal gas (helium) venting from the cube clearly exhibited g-jitter effects that were similar to the experi-

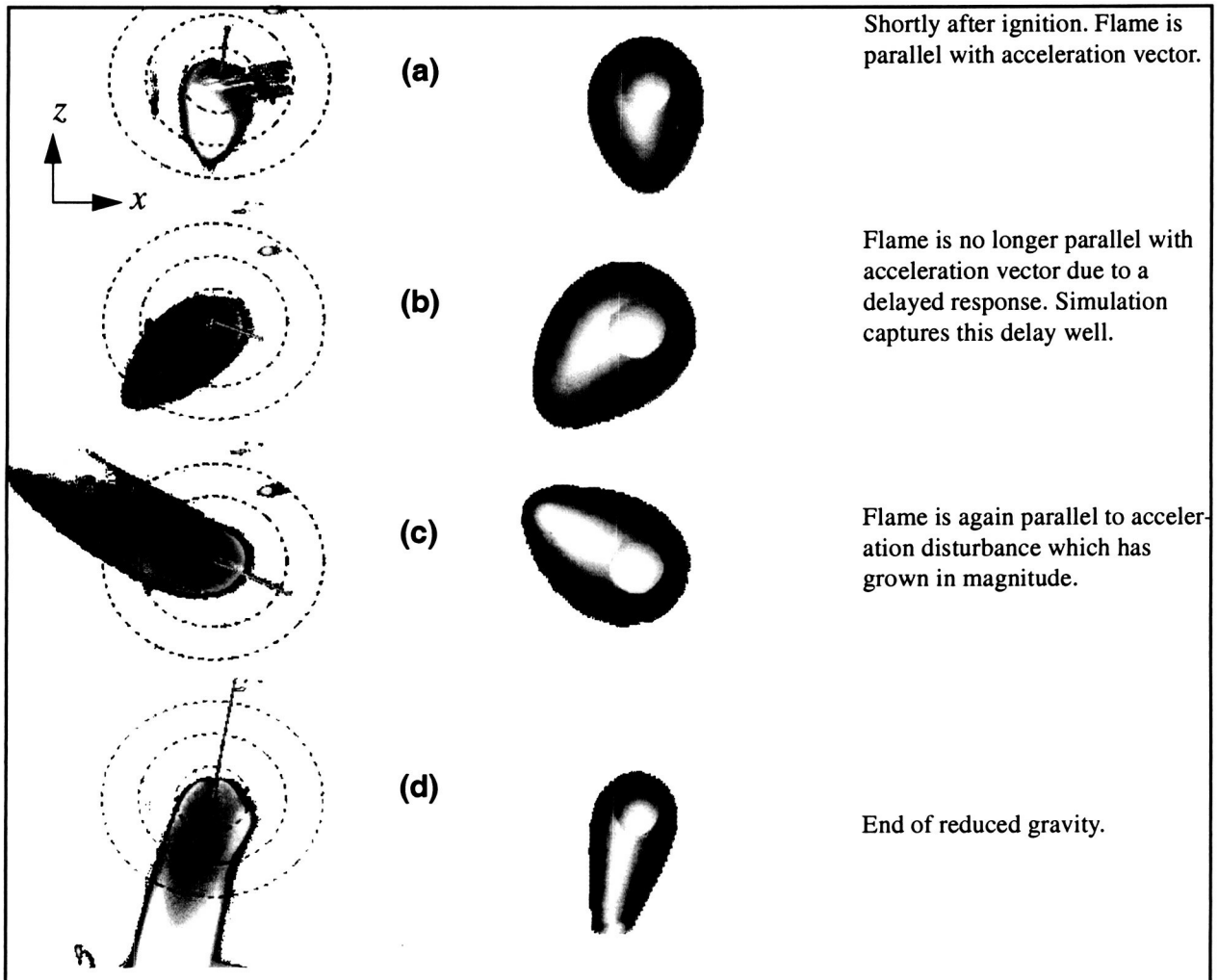

FIGURE 10: Results of experimental [Struk *et al.*, (1996)video images on left] and simulated (snap shots of temperature isosurfaces on right) flames. Experimental flames are from an n-decane droplet formed from n-decane liquid issuing from a porous 5 mm sphere. Simulated flames are from n-decane gas issuing from a 5 mm cube. Four times, increasing downward from (a) to (d), are shown. Each dotted circle denotes an acceleration magnitude: first circle = 0.01 ge, second circle = 0.02 ge, etc.; the line in the experimental figures shows the direction of acceleration in the plane of the video (x-z plane) frame. Time history of acceleration disturbance is plotted in Fig. 9. Simulations used ~ 1 mm uniform grid, ~ 2000 grid pts (45x45x45) over 50x50x50 mm domain; required 46 CPU hours (60979 time steps for 19 s) on a R12000, 270 MHz SGI Octane

mental observations. Note that animations of the simulated and experimental flames, side by side, can be viewed on a web page for this project Mell *et al.* (2003a).

In experiments attached to the airframe, the orientation of the *g*–jitter was such that numerical simulations of *g*–jitter effects need to be three-dimensional (as opposed to axially–symmetric, for example). Acceleration disturbances can also be directionally dependent in sounding rockets (Ross and Espinoza, 1997). The peak disturbances in the sounding rocket and the experiments

bolted to the airframe are similar in magnitude but are of much shorter duration in the sounding rocket.

5 Application to assessing ISS limit for a transient acceleration disturbance

A number of design requirements that specify acceptable limits of acceleration disturbances have been developed (Feikema, 2001; NASA, 1996). One of these requirements is that an individual transient acceleration disturbance be less than or equal to 1000 micro-g per axis and the integrated transient acceleration limit is less than or equal to 10 micro-g seconds per axis within any 10 s time interval. The validity, within the context of numerical simulations, of this limit was tested using 3-D simulations of a spherical diffusion flame subjected to successively weaker acceleration disturbances. The starting point was the disturbance level of $\boldsymbol{g} = (0.005, 0, 0.005)g_e$that was present in Feikema's (2001) free-floating KC-135 experiments (discussed in Sec. 4.2, see Fig. 8). Successive simulations were made, each with the acceleration decreased by an order magnitude from the previous simulation. Results were obtained from well resolved direct numerical simulation with 1.2 mm uniform grids, 128x64x128 grid cells, open boundary conditions, and no radiation solver; 10 cpu hours needed for 1.4s on 1.7 GHz P4.

The integrated limit of 10 micro-g seconds implies that a constant acceleration disturbance of magnitude g_d and duration t_d must be related as

$$g_d \leq \frac{0.01\,\mathrm{mg}\cdot\mathrm{s}}{t_d}, \tag{1}$$

in order for the limit to be satisfied. For the case of Feikema's free-floating experiment (g_d = 5 mg) the limit was exceeded in 2 ms. Simulations with g_d = 0.5 mg also clearly displayed the effect of the acceleration disturbance, results were similar to Fig. 8 but after 2 s of simulation. For the case of $\boldsymbol{g}$ = (0.05 mg, 0 mg, 0.05 mg), which from Eq. (1) implies t_d = 0.25 s, the temperature is shown in Fig. 11a. There is no discernible influence of the imposed acceleration on the flame's spherical symmetry in Fig. 11a (e.g., compare to Fig. 8). However, if the temperature field in Fig. 11a is compared point by point over the computational grid to the temperature field from a simulation with no acceleration disturbance, $\boldsymbol{g}$ = 0 mg, then changes up to 9% in the temperature field are seen. This is shown in Fig. 11b by the line contours.

Note that the largest deviation from the zero g case does not occur near the flame (where the deviation is ~ 1%, see Fig. 11b); in fact they occur at nearly ambient temperatures. This is probably due to stabilizing effects of the forced fuel flow from the burner and the (opposite in direction) expansion velocity from the combustion. This stabilization does not occur at the 'wings' of the flame which are then more susceptible to buoyancy effects. This is discussed further in Sec. 6 below in the discussion regarding simulations using the hard mounted SAMS2 acceleration data.

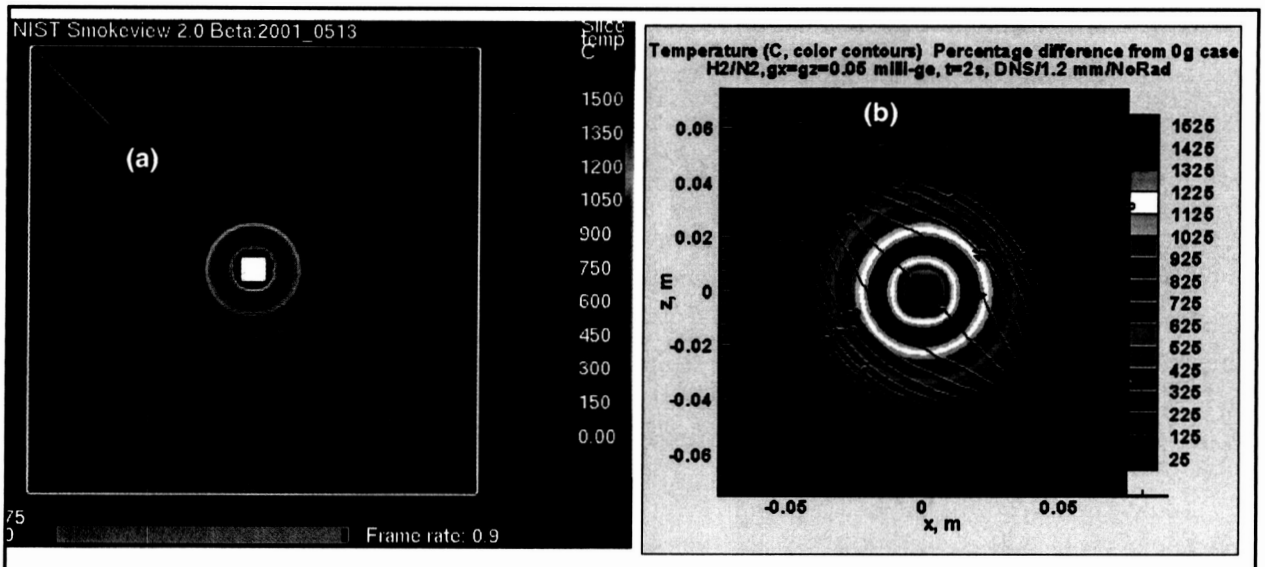

FIGURE 11: **(a)** Temperature contours of a simulated hydrogen flame after 2 s in a constant $\boldsymbol{g}$ = (0.05 mg, 0 mg, 0.05 mg) acceleration environment. No break in the spherical symmetry is discernible. **(b)** Same flame as in figure (a), color contours of temperature and line contour of the percentage difference between the flame subjected to $\boldsymbol{g}$ = (0.05 mg, 0 mg, 0.05 mg) for 2 s and to $\boldsymbol{g}$ = 0.

Decreasing the magnitude of the acceleration disturbance by another order of magnitude to $\boldsymbol{g}$ = (0.0005 mg, 0 mg, 0.0005 mg), so that t_d = 2.5 s, the percentage change from the $\boldsymbol{g}$ = 0 mg case is under 1% at t = 2 s. This seems to be an acceptable amount of disturbance. Note that since the time at which the disturbance is assessed, t = 2 s, is smaller than t_d = 2.5 s this also suggests the design limit on integrated acceleration disturbances of 10 micro-g seconds or less is a good limit (assuming the behavior of the flames is adequately predicted by the simulation).

6 Simulations with measured acceleration disturbances on the ISS

The background acceleration environment is routinely measured on the ISS. In this section results from simulations of spherical diffusion flames with different measured acceleration histories are presented. The goal is to assess the influence of the acceleration disturbance on flame dynamics by comparing results from simulations with a nonzero acceleration disturbance to results with $\boldsymbol{g}$ = 0.

The computer simulations discussed in this section used the mixture fraction based flame sheet combustion model, were fully three-dimensional (no symmetry planes), and transient. Uniform computational grids 4 mm resolution (64x64x128 grid points) covered a 25 cm by 25 cm wide by 50 cm high volume; 20 s of simulated real time required 8 cpu hours and 4432 time steps on a Pentium 4, 1.7 GHz processor. The fuel gas mixture was 60%H_2-40%N_2 (by mole fraction) and exited a 12 mm on a side cube shaped burner at 1.9 cm/s. The burner temperature was held fixed at 90 C (average temperature of Tse *et al.* (2001) spherical burner). Thermal radiation transfer was not implemented (the flame is adiabatic). The entire GIFFTS experimental domain (see Fig. 1)

was simulated (although the cylindrical volume is approximated by a rectangular volume). The walls were thermally thick as were any experimental structures in the interior of the volume, such as the support platform seen in Fig. 1. The coarse resolution of these simulations results in more rapid flame growth and lower temperatures. However, the same series of simulations with a step-wise decrease in the magnitude of the acceleration disturbance that was conducted in the previous section, for much better resolved flames, was also conducted using the coarse grid. It was found that the flame on the coarse grid was just as sensitive to acceleration disturbances.

Three different acceleration measurements were used: with the Active Rack Isolation System (ARIS) in both active and idle (in which case it acted as a passive isolation system) modes and from measurement of a sensor hard mounted on the experimental rig support structure during light crew activity. The time histories of the components of the acceleration vector for each of these cases are shown in Fig. 12. Note that the amplitude of the acceleration levels when ARIS is active is an order of magnitude smaller than when ARIS is idle. Also there is a comparative absence of low frequency components, which are know to be more disruptive than higher frequencies. The hard mounted measurements are an order of magnitude larger than for the ARIS idle case. The larger magnitude disturbances, however, are at higher frequencies.

The 3-D visualization tool (Smokeview, [Forney *et al.*, 2003]) was used to compare flame shapes from simulations with and without the support surface which is located 10 cm from the burner (see Fig. 1). The presence of this support surface caused the flame to lose spherical symmetry along the z-axis after a few seconds. The effects of g-jitter on spherical symmetry were isolated from the effects of the support surface by comparing results with g-jitter to those with 0 g (both of which have the support surface). This is done below.

Figure 13 shows color contours of the temperature and line contours of the percentage difference from the $\boldsymbol{g} = 0$ case when ARIS is idle. The presence of the support structure is clearly seen by the flattening of the temperature contours at the top boundary of the flame in Fig. 13b. Note that an actual flame would most likely not be this large at 10 s because the coarse grid resolutions of this simulation increase the rate of the flame growth. The deviation from the $\boldsymbol{g} = 0$ case in Fig. 13a (t = 5 s) is 2.5% or less and in Fig. 13b (t = 10 s) is 3% or less. Based on the results in Sec. 5 this is probably an acceptable amount of disturbance. Simulations with the ARIS active acceleration data of Fig. 12a were also conducted but are not plotted here. The flame for this case was even less affected by the acceleration disturbance.

Results from the simulation with the hard mounted sensor measurements during light crew activity (i.e., $\boldsymbol{g}$ from Fig. 12c) are shown in Fig. 14. The flame is mainly disturbed along the x-axis which is the orientation of the largest acceleration disturbance (see Fig. 12c). Note that in a central region, bounded by the temperature peaks, the 0g and ISS results are identical. It's only in the outer 'wings' of the temperature profile that there's deviation from the 0 g case. A probable reason for this can be inferred from Fig. 15 which shows profiles of the temperature (using measured and zero $\boldsymbol{g}$), the horizontal velocity and the heat release per unit volume (from the case with measure $\boldsymbol{g}$). Note that temperatures for the 0 g case are lower to the right of the burner and higher to the left

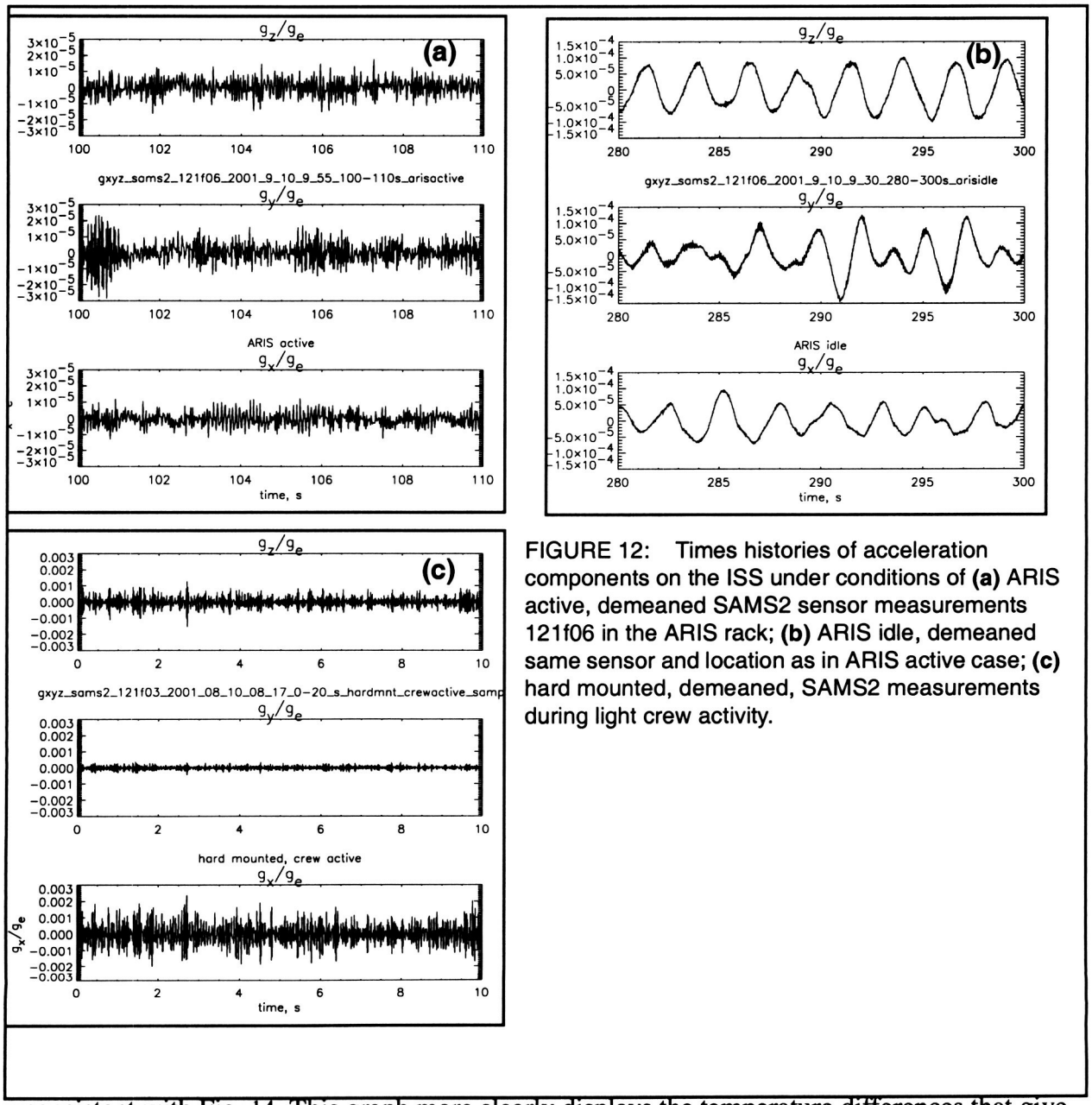

FIGURE 12: Times histories of acceleration components on the ISS under conditions of **(a)** ARIS active, demeaned SAMS2 sensor measurements 121f06 in the ARIS rack; **(b)** ARIS idle, demeaned same sensor and location as in ARIS active case; **(c)** hard mounted, demeaned, SAMS2 measurements during light crew activity.

– consistent with Fig. 14. This graph more clearly displays the temperature differences that give rise to the percentages seen in Fig. 14. The flow of fuel from the burner (+/- 1.9 cm/s) dominates in the central region. This flow and flow (in the opposite direction) due to thermal expansion near the reaction zone stabilize the 'inner' flame region. In a premixed spherical flame (no burner) velocities would be much smaller, probably resulting in a flame that's more sensitive to acceleration disturbances. This is seen in here in the 'outer' flame region, just outside of the peak heat release, where the velocity is an order of magnitude smaller than it is near the burner.

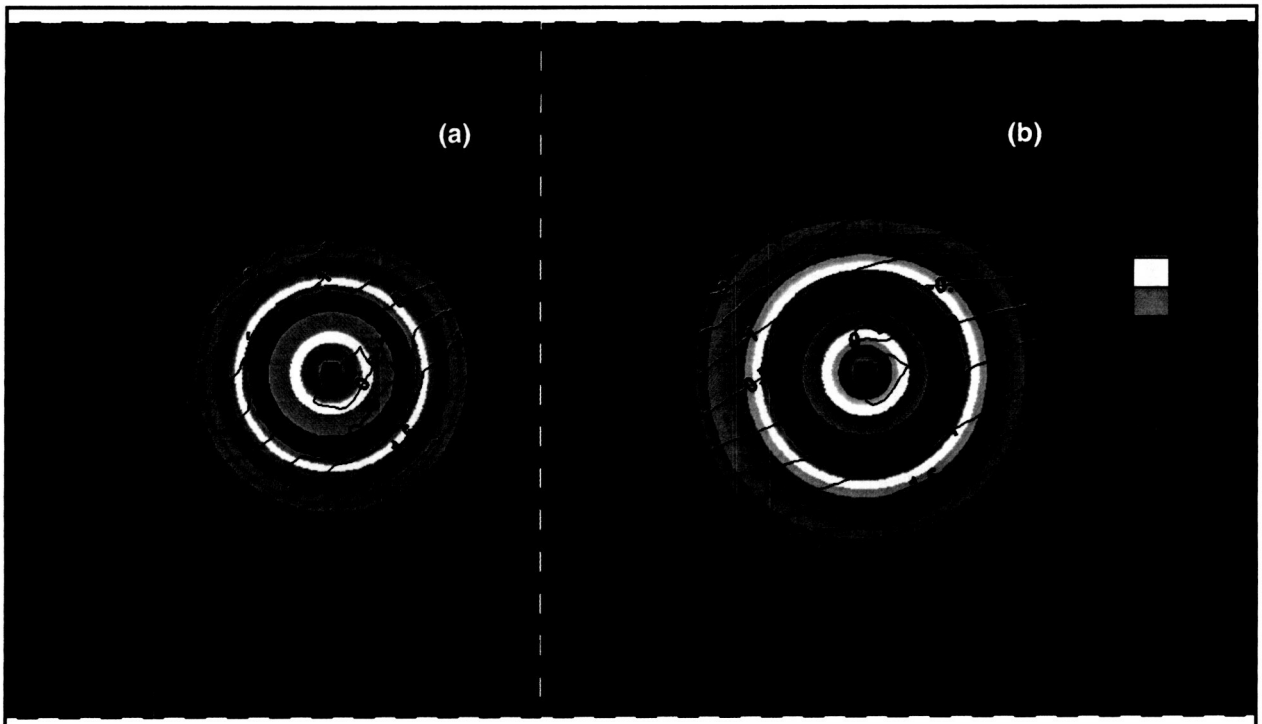

FIGURE 13: Case when ARIS is idle, Fig. 12b. Color contours of temperature (C) and line contours of the percentage difference from the zero g case are both shown. **(a)** Results for $t = 5$ s. **(b)** Results for $t = 10$ s.

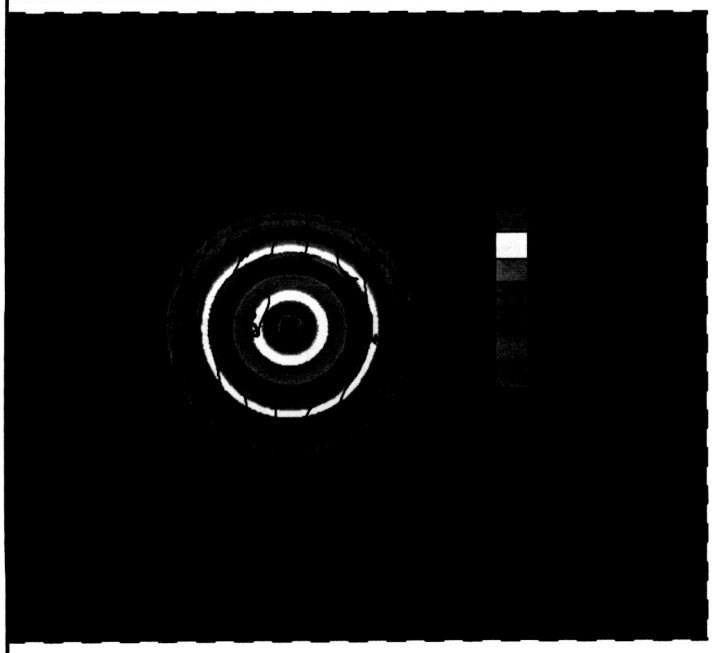

FIGURE 14: Simulation results for the case when $\boldsymbol{g}(t)$ is from a hard mounted sensor during light crew activity. Color contours of temperature and line contours of the percentage difference from the $\boldsymbol{g} = 0$ case are both shown at $t = 5$ s.

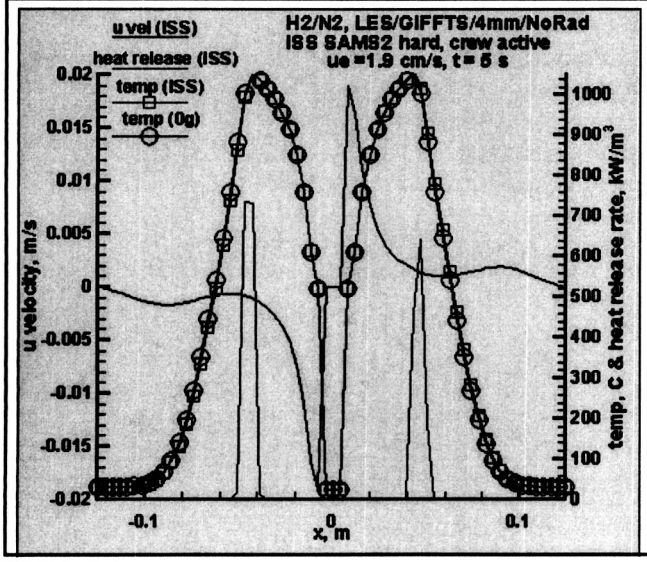

FIGURE 15: Temperature profiles across the middle of the flame in Fig. 14. Results using both $g = 0$ (circles) and g from the hard mounted SAMS2 acceleration measurements with the crew active (squares) are shown. Profiles for the velocity (in the x direction) and the heat release per unit volume for the case with measure g are also shown.

7 Simulations with predicted acceleration disturbances on the ISS

A number of simulations were run to assess the need for an Active Rack Isolation System to isolate combustion experiments from acceleration disturbances on the ISS. The results of some of these simulations were presented in the previous section. Another set of simulations used acceleration disturbances obtained from finite element simulations of the fully complete ISS structure operating with all known sources of acceleration disturbance "turned on" (e.g., control moment gyroscopes, ergometers, solar panel joints) and without any isolation systems present. These acceleration disturbances are based on a Non Isolated Rack Assessment (NIRA) and is a prediction of the acceleration environment in Columbus Laboratory after completion of the ISS assembly and during the 'microgravity' periods. The NIRA 'sky line' vibratory assessment includes the disturbance sources in the structural dynamic and vibro-acoustic range (0.01 through 300 Hz) and results from Boeing/NASA-JSC models of the assembled ISS with the addition of forcing functions. The analysis assumes 1% damping applied to the 100 second averaged, root-mean-square acceleration magnitude at the center frequencies of the one-third octave bands from 0.01 through 300 Hz.

Figure 16 shows NIRA derived information of the acceleration environment in the ISS. Figure 16a is a spectral plot of the NIRA prediction of the magnitude of the acceleration. Figure 16b is ten seconds of the acceleration time history obtained by a sum of sinusoids whose frequencies and amplitudes are obtained from a modification of the NIRA prediction in Fig. 16a. Frequencies up to 100 Hz were used. Note that the full range of frequencies covered by the NIRA prediction were not plotted in Fig. 16a . Using higher frequencies made little difference in the derived acceleration time history since their amplitude was two orders of magnitude lower (not shown) than the 10^{-2} g_e peak at ~ 3 Hz easily seen in Fig. 16a. Figure 16c shows (dotted line) what portion of the original NIRA data in Fig. 16a was actually used to compute the time series in Fig. 16b. The solid line in

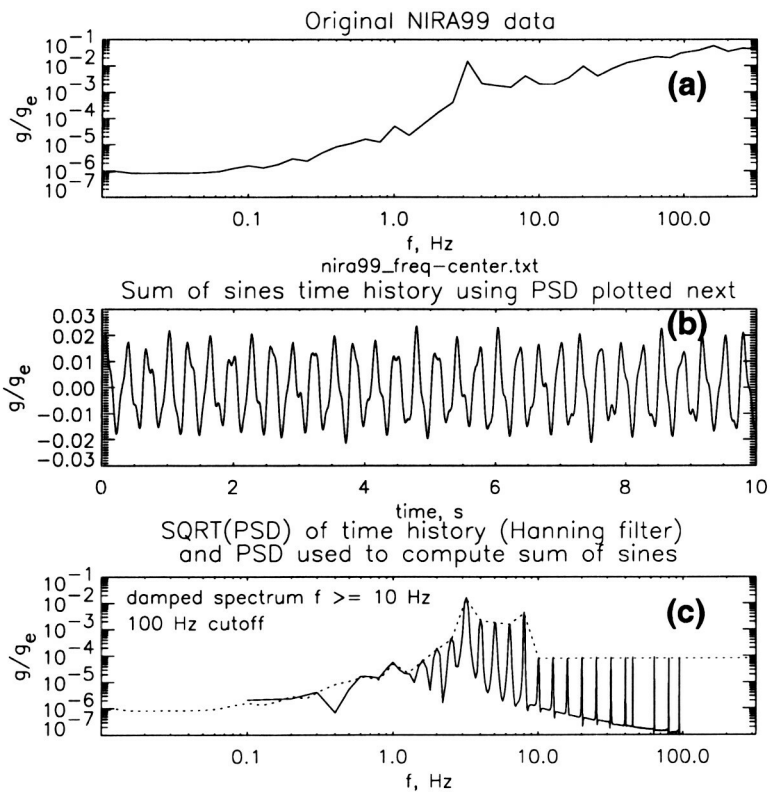

FIGURE 16: Acceleration data derived from a NIRA prediction. **(a)** A spectral plot of the NIRA prediction of the acceleration. **(b)** a 10 s acceleration time history derived from a modified form of figure (a). **(c)** shows the portion of the NIRA data figure (a) that was used to compute the time series (dotted line) plotted in figure (b). See the text for more details.

Fig. 16c shows the result of using a Hanning filter on the time history and then performing an FFT, computing the power spectral density (PSD) and plotting its square root. The lower frequencies were lost due to the Hanning filter. At all other frequencies the square root of the PSD agree well with the original NIRA data. The original NIRA data was damped for frequencies > 10 Hz because at the time of this run the validity of the amplitudes at higher frequencies was in question. Also, frequencies higher than 100 Hz were cutoff. The reason for the 100 Hz cutoff is to avoid aliasing by the simulation code which effectively samples the time history at 200 Hz. Note that the 3 Hz peak dominates the time history behavior in Fig. 16b.

The level of peak acceleration disturbance (+/- 0.02 g_e) in Fig. 16b is comparable to bolted down experiments in the DC-9 (see Fig. 9). And an order of magnitude larger than the hard mounted (light crew activity) case of Fig. 12c. Note, however, that the accelerations in the hard mounted case are at higher frequencies.

The time history in Fig. 16b was used to represent the g_z component of the acceleration vector, $\boldsymbol{g} = (0, 0, g_{NIRA})$, in a simulation of a spherical hydrogen diffusion flame. The properties of the simulation (i.e., grid resolution, combustion model, etc.) were the same as the simulations conduction in Sec. 6 above (see the simulation description at the beginning of Sec. 6). Note, however, that the simulations in Sec. 6 used measured acceleration data for all three components of the acceleration vector. In Fig. 17 the results of the simulation using $\boldsymbol{g} = (0, 0, g_{NIRA})$ are plotted in

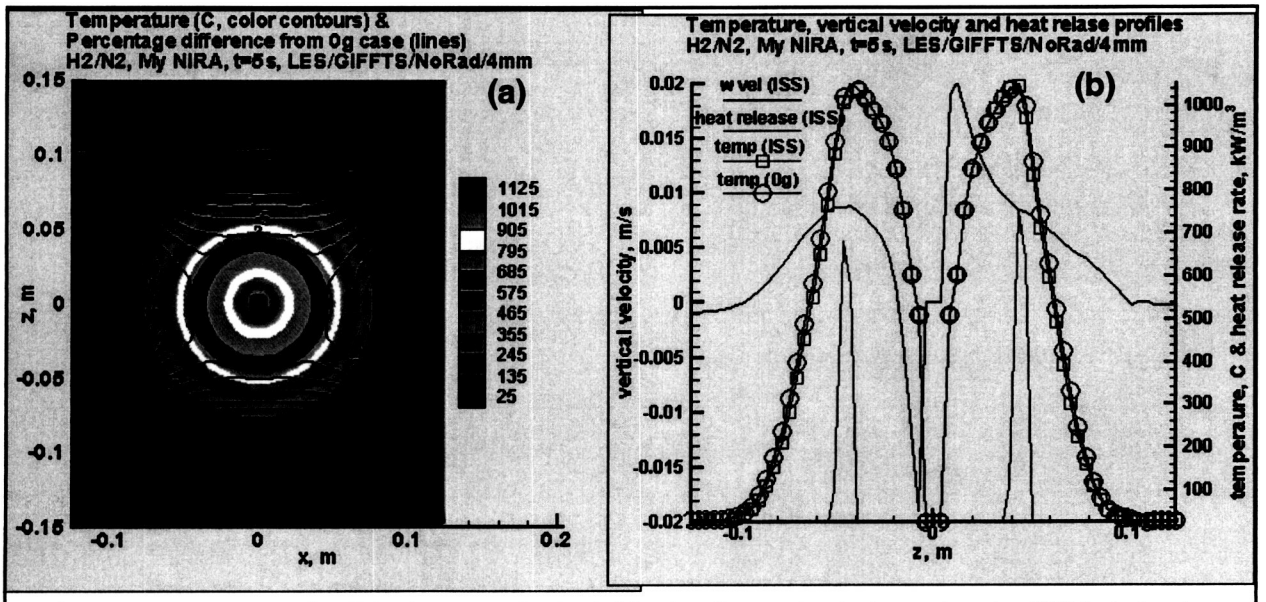

FIGURE 17: Results of 3-D hydrogen spherical diffusion flame simulation using the NIRA derived acceleration time history $\boldsymbol{g} = (0, 0, g_{NIRA})$ where $g_{NIRA}(t)$ is from Fig. 16b. **(a)** Shows color contours of the temperature field and line contours of the percentage deviation of the temperature from an identical simulation with $\boldsymbol{g} = 0$. Maximum deviation magnitude is 11% at the bottom of the figure. **(b)** Vertical profiles of the temperature (squares from g_{NIRA} and circles from $\boldsymbol{g}$=0 simulations), vertical velocity, and heat release rate per unit volume. Time is $t = 5$ s.

the same manner as with measured acceleration in Figs. 14 and 15 above. That is, color contours of temperature for the NIRA case and line contours for the percentage difference in the temperature between the NIRA case and the $\boldsymbol{g} = 0$ case are shown in Fig. 17a at $t = 5$ s. Deviations from the $\boldsymbol{g} = 0$ case are symmetric in the x-direction but asymmetric in the z-direction (as expected). The deviation from the $\boldsymbol{g} = 0$ case is twice that of the other ISS cases considered (ARIS idle, Fig. 13; hard mounted with light crew activity, Fig. 14).

Figure 17b shows vertical profiles of temperature (NIRA and $\boldsymbol{g}$=0 simulations), vertical velocity (NIRA simulation only) and heat release rate (NIRA simulation only). All quantities are asymmetric due to the acceleration disturbance. The asymmetry is especially pronounced (compare to same figure for hard mounted case, Fig. 15) for the vertical velocity.

In animations of the simulation corresponding to Figs. 16 and 17 clearly the flame clearly oscillated vertically its spreads outward from the burner. The direct url link to these animations is at Mell (2003c). This oscillation was though to be due to the peak at 3 Hz in the NIRA prediction. This contribution to the acceleration is due to an ergometer.

In order to test whether the acceleration disturbance at 3 Hz was the source of the flame's oscillatory behavior it was removed from the NIRA spectrum in Fig. 16a and a new acceleration time history was computed and used in a spherical flame simulation. Figure 18a shows the original NIRA prediction and the dotted line in Fig. 18c shows its modified form without the peak at 3 Hz. This modified spectrum, out to 50 Hz, was used to obtain the acceleration time history shown in

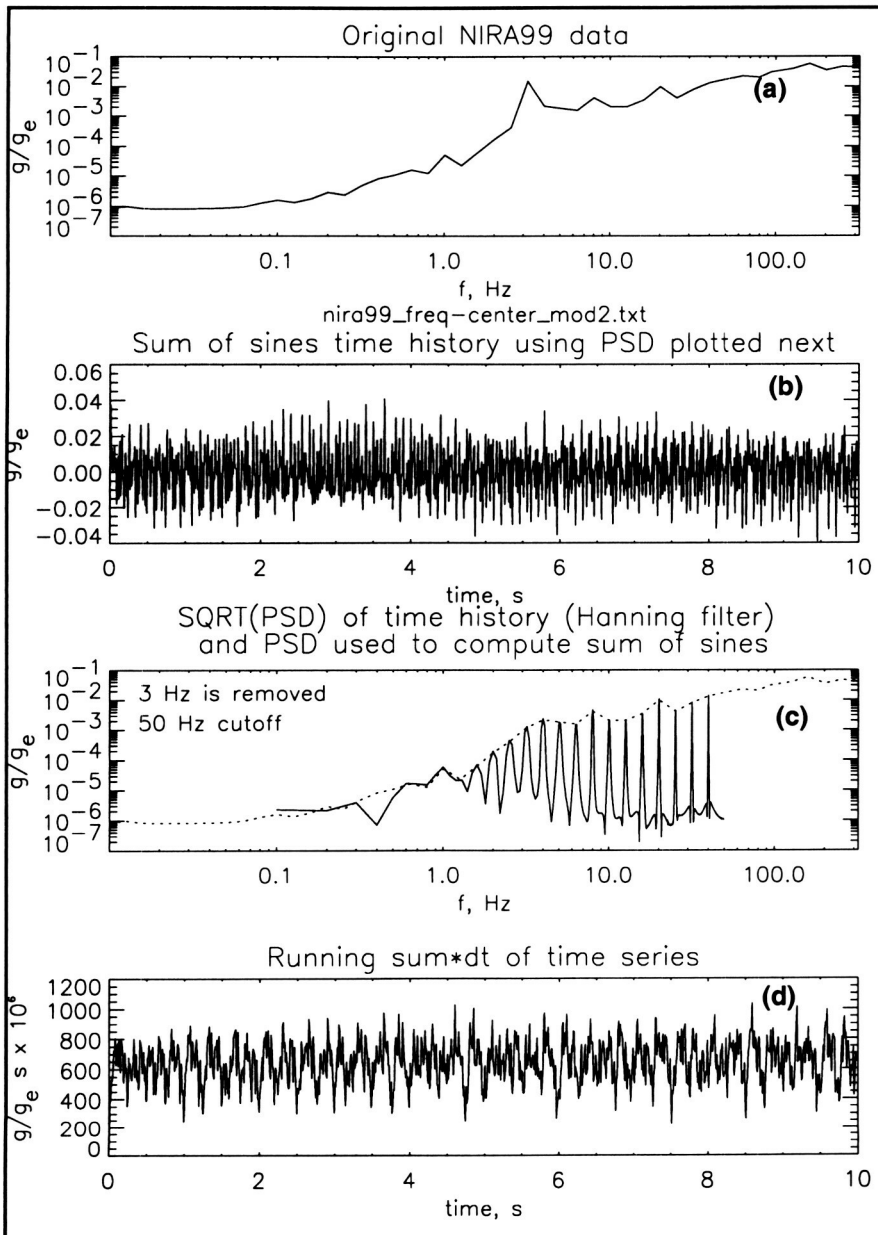

FIGURE 18: NIRA derived acceleration. **(a)** Original NIRA prediction. **(b)** Time series of acceleration derived from the modified NIRA spectrum of (c) using a sum of sines. **(c)** Modified form of the original NIRA spectrum in (a) with the ~ 3 Hz peak is removed is shown as a dotted line. This spectrum out to 50 Hz is used to derive the time series in (b). **(d)** Running sum of the acceleration time series multiplied by *dt* in (b). This is a running check of whether or not the acceleration disturbance meets the integrated transient disturbance limit. The vertical axis is in units of micro-g.

Fig. 18c. As before, this acceleration time history was used for g_z in a new simulation. No flame oscillation was observed in the simulation.

However, animations clearly showed the flame moving downward. The source of this disturbance can be identified by checking to see if the acceleration time history meets the criteria of a 10 micro-g seconds integrated disturbance. Figure 18d is a time history plot of the running sum:

$$\int_0^t \frac{g_{\mathrm{NIRA}}}{g_{\mathrm{e}}} dt = \sum_i \frac{g_{\mathrm{NIRA}}}{g_{\mathrm{e}}} \Delta t \leq 10 \text{ micro-g seconds for } t \leq 10 \text{ s}. \qquad (2)$$

As stated in Eq. (2) this running sum must be less than or equal to 10 micro-g seconds over a time interval of 10 s or less. It is clear from Fig. 18d that the flame is subjected to a net acceleration disturbance in the positive z direction. This disturbance does not meet the integrated transient limit requirement. Note the vertical axis in Fig. 18d is in units of micro-g. This undesirable acceleration disturbance is the result of using a sum of sines based on a spectrum which has a broad range of frequencies with amplitudes large enough to affect the flame. In the previous simulation case, because the 3 Hz peak in the modified NIRA99 spectrum sufficiently dominated the acceleration time history, this transient acceleration was not a factor .

The results of this series of simulations suggested a passive isolation system and appropriate scheduling of crew activity would provide a sufficiently "quiet" acceleration environment for spherical diffusion flames.

8 References

Baumann, E. (2003), NASA Glenn Research Center, personal communication.

Feikema, D. (2001) "Effects of Acceleration Environment on the Stability of Spherical Diffusion Flames," presented at the *2nd Joint Meeting of the U.S. Sections of the Combustion Institute*, Oakland, CA, March 26-29, 2001.

Forney, G.P. and McGrattan, K.B. (2003) "User's Guide for Smokeview Version 3.1: A Tool for Visualizing Fire Dynamics Simulation Data," NISTIR 6980; 57 p. April 2003

Grosshandler, W. (1993) "RadCal: A Narrow Band Model for Radiation Calculations in a Combustion Environ-ment," NIST Technical Note (TN 1402), National Institute of Standards and Technology, Gaithersburg, Maryland 20899.

Mell, W.E. and Takashi, T. (1998) "Dimensional effects on the transition from ignition to flame spread in microgravity," *Proceeding of the Combustion Institute*, **27**, pp. 2635-2641

Mell, W.E., Olson, S.L., and Takashi, T. (2000) "Flame spread along free edges of thermally thin samples in microgravity," *Proceeding of the Combustion Institute*, **28**, pp.2843-2849.

Mell, W.E., McGrattan, K.B., and Baum, H.R., (2003a), web page for project, as of July 6, 2003, http://ruddy-sgi.crsim.utah.edu/~ruddy/WORK/NASA/G-JITTER/g-jit_public.html

Mell, W.E., McGrattan, K.B., and Baum, H.R., (2003b) "*g*-jitter effects on spherical diffusion flames," to be submitted early Fall 2003, *Microgravity Science and Technology.*

Mell, W.E. (2003c) link to animation of simulation corresponding to Figs. 16 and 17: http://ruddy-sgi.crsim.utah.edu/~ruddy/WORK/NASA/G-JITTER/MPG_MOVIES/GIFFTS_YH20.1_MyNIRA99_64x64x128.mpg

McKinnon, T., Abbud, A., and Riedel, N. (2003) "Water Mist Suppression Experiment", home page: http://microgravity.grc.nasa.gov/combustion/mist/mist_index.htm (as of July 7, 2003).

McGrattan, K.B., Kashiwagi, T., Baum, H.R., and Olson, S.L. (1996) "Effects of ignition and wind on the transition to flame spread in a microgravity environment," *Combustion and Flame*, **106**, pp. 377-391.

McGrattan, K.B., Baum, H.R., Rehm, R.G., Hamins, A., Forney, G.P., Floyd, J.E. and Hostikka, S. (2002) "Fire Dynamics Simulator (Version 2) - Technical Reference Guide," *NIST Internal Report*, NISTIR 6782 2002 ed., National Institute of Standards and Technology, November 2002.

Miyasak, K. and Law, C.K. (1981) "Combustion of strongly-interacting linear droplet arrays," *Proc. Combustion Institue,* **18**, pp. 282-292.

Nakabe, K., McGrattan, K.B., Kashiwagi, T., Baum, H.R., Yamashita, H. and Kushida, G. (1994) "Ignition and transition ot flame spread over a thermally thin cellulosic sheet in a microgravity enviornment," *Combustion and Flame,* **98**, pp. 361-374.

NASA (1996) SSP 410000 revision E, "The Microgravity Plan," paragraph 6.2.5, July 1996.

Rehm, R.G. and Baum, H.B (1978), "The Equations of Motion for Thermally Driven, Buoyant Flows," *Journal of Research of the National Bureau of Standards*, **83**

Ross, H. and Espinoza, B. (1997) NASA Lewis Research Center, personal communication; data is from recent sounding rocket experiments of flame spread across liquids. See Ross, H.D. and Miller, F.J., "Flame Spread Across Liquids," *Proceedings of the Fourth International Microgravity Combustion Workshop*, Cleveland, OH, May 19–21, 1997, pp. 375–380.

Struk, P.M., Dietrich, D.L. and T'ien, J.S., (1996) "Large Droplet Combustion Experiment Using Porous Spheres Conducted in Reduced Gravity Aboard an Aircraft – Extinction and the Effects of g–jitter," *Microgravity Sci. Technol.*, Vol. 9, No. 2, pp. 106–116.

Tse, S.D., Zhu, D.L., Sung, C.J., and Law, C.K. (1999) "Microgravity Burner--Generated Spherical Diffusion Flames: Experiment and Computation," *AIAA Aerospace Sciences Meeting and Exhibit*, AIAA-99-0585.

Tse, S.D., Zhu, D.L., Sung, C.J., and Law, C.K. (2001) "Microgravity Burner--Generated Spherical Diffusion Flames: Experiment and Computation," *Combustion and Flame*, **125,** pp. 1265-1278.

Tse, S.D. (2003), Rutgers, State University of New Jersey, personal communication.

Westbrook, C.K. and Dryer, F.L. (1981) "Simplified reaction mechanisms for the oxidation of hydrocarbon fuels in flames," *Combustion Science and Technology*, **27**, pp. 31-43.